Biomaterials 34 (2013) 5138–5148

Contents lists available at SciVerse ScienceDirect

Biomaterials

journal homepage: www.elsevier.com/locate/biomaterials

The influence of the penetrating peptide iRGD on the effect of paclitaxel-loaded MT1-AF7p-conjugated nanoparticles on glioma cells

Guangzhi Gu [a], Xiaoling Gao [b], Quanyin Hu [a], Ting Kang [a], Zhongyang Liu [a], Mengyin Jiang [c], Deyu Miao [c], Qingxiang Song [b], Lei Yao [b], Yifan Tu [a], Zhiqing Pang [a], Hongzhuan Chen [b], Xinguo Jiang [a], Jun Chen [a,*]

[a] Key Laboratory of Smart Drug Delivery, Ministry of Education & PLA, School of Pharmacy, Fudan University, Lane 826, Zhangheng Road, Shanghai 201203, PR China
[b] Department of Pharmacology, Institute of Medical Sciences, Shanghai Jiaotong University School of Medicine, 280 South Chongqing Road, Shanghai 200025, PR China
[c] School of Pharmacy, Shandong University of Traditional Chinese Medicine, Jinan, Shandong, PR China

ARTICLE INFO

Article history:
Received 17 January 2013
Accepted 13 March 2013
Available online 9 April 2013

Keywords:
MT1-AF7p
iRGD
Glioblastoma
Co-administration
Paclitaxel
Nanoparticle

ABSTRACT

Low permeability across the blood–brain tumor barrier (BTB) and poor penetration into the glioma parenchyma represent key obstacles for anti-glioblastoma drug delivery. In this study, MT1-AF7p peptide, which presents high binding affinity to membrane type-1 matrix metalloproteinase (MT1-MMP) that over-expressed on both angiogenic blood vessels and glioma cells, was employed to decorate the paclitaxel-loaded PEG-PLA nanoparticles (MT1-NP-PTX) to mediate glioblastoma targeting. Tumor-homing and penetrating peptide iRGD was co-administrated to further facilitate nanoparticles extravasation from the tumor vessels and penetration into the glioma parenchyma. MT1-NP-PTX showed satisfactory encapsulated efficiency, loading capacity and size distribution. In C6 glioma cells, MT1-NP was found to exhibit significantly enhanced cellular accumulation than that of unmodified NP via both energy-dependent macropinocytosis and lipid raft-mediated endocytosis. The anti-proliferative and apoptosis-induction activity of PTX was significantly enhanced following its encapsulation in MT1-NP. In vivo imaging and glioma distribution together confirmed that MT1-AF7p functionalization and iRGD co-administration significantly improved the nanoparticles extravasation across BTB and accumulation in glioma parenchyma. Furthermore, *in vitro* C6 glioma spheroid assays evidenced that MT1-NP effectively penetrated into the glioma spheroids and significantly improved the growth inhibitory effects of loaded PTX on glioma spheroids. More importantly, the median survival time of those nude mice bearing intracranial C6 glioma received MT1-NP-PTX and iRGD combination regimen was 60 days, significantly longer than that of other groups. The findings suggested that the BTB/glioma cells dual-targeting DDS co-administrated with iRGD peptide might provide a both practical and feasible solution to highly efficient anti-glioblastoma drug delivery.

1. Introduction

Glioblastoma multiforme (GBM) is the most common malignant primary brain tumor in adults and among the most lethal of all cancers. Despite surgical and medical advancements, the prognosis for patients with glioblastoma still remains dismal, with a median survival of only 14.6 months [1]. Glioma cells have a remarkable capacity to disperse widely throughout the brain, making complete surgical resection impossible, and are responsible for tumor recurrence and ultimate patient demise [2]. Chemotherapy is indispensable for glioblastoma treatment after surgery [3], but only achieves very limit benefits due to the insufficient drug accumulation in the glioma and the serious side effects induced by nonspecific biodistribution [4,5]. Although in most cases of glioblastomas, the blood–brain barrier (BBB) is compromised by angiogenesis and tumor growth, the thereafter formed blood–brain tumor barrier (BTB) which resides between the brain tumor cells and microvessels, still poses a major hurdle to the delivery of anticancer drug into the glioma sites [6–8]. Moreover, the multiple layers of tumor cells also pose a major obstacle that prevents anticancer drugs from reaching cells that reside away from the

* Corresponding author. Tel.: +86 21 51980066.
E-mail addresses: chenjun@fudan.edu.cn, chenjun_1974@yahoo.com.cn (J. Chen).

0142-9612/$ – see front matter © 2013 Elsevier Ltd. All rights reserved.
http://dx.doi.org/10.1016/j.biomaterials.2013.03.036

blood vessel, leading to drug resistance and failure in chemotherapy [9–11]. Accordingly, development of an effective drug delivery system (DDS) possessing the ability to obtain extensive extravasation and specific accumulation at the glioblastoma foci but not the peripheral tissues and healthy brain tissue is of ever-increasing importance for anti-glioblastoma drug delivery.

Nanoparticulate carriers, especially biodegradable polymeric nanoparticles are playing an increasingly important role in developing more effective brain tumor treatments [12]. Active targeting DDS, generally mediated by the presence of specific molecules on the outer surfaces of the nanoparticles, have been widely exploited to elevate drug delivery to glioblastoma [13,14]. Since BTB constitutes the main barrier in glioblastoma, BTB/glioma cells dual-targeting drug delivery is desirable for anti-glioblastoma therapy [15,16]. Membrane type-1 matrix metalloproteinase (MT1-MMP), also referred to as MMP-14, was of central importance in glioma invasion and angiogenesis [17–19]. It is predominantly expressed in angiogenic blood vessels and glioma cells [20,21], and increased with the elevation of glioma grade. It can activate MMP-2, up-regulate vascular endothelial growth factor (VEGF), and also possesses proteolytic activity towards extracellular matrix (ECM) molecules, independent of MMP-2 [19,22]. These backgrounds made MT1-MMP an ideal target for anti-glioblastoma drug delivery [23]. MT1-AF7p peptide (HWKHLHNTKTFL), identified via phage display, possesses high specificity to MT1-MMP [24]. More importantly, MT1-AF7p exhibits a fairly high affinity to MT1-MMP (apparent K_d = 47.41 nM), suggesting MT1-AF7p as an attractive ligand for MT1-MMP targeting. Here we speculated that MT1-AF7p might serve as a dual-targeting ligand to be conjugated to nanoparticles for mediating their BTB penetration and glioma cells-targeting.

Despite active targeting, nanoparticulate DDS that can extravasate from tumor vessels and accumulate in the glioma sites is still highly restricted by high interstitial fluid pressure and binding-site barrier [25]. Interstitial fluid pressure, which is much higher in tumor than that in normal tissue, forms a barrier to transcapillary transport [26]. Binding-site barrier, which was induced by the strong interaction between active targeting nanoparticles and their targets, also greatly inhibited the extravascular transport of the nanoparticles and blocked the penetration of nanoparticles into the tumor interstitium [27]. Recent findings witnessed the tumor-specific vascular extravasation and tissue penetration activity of iRGD that contains an RGD motif with a protease site and a cryptic Cend Rule (CendR) motif (R/KXXR/K). The RGD motif of iRGD firstly binds to αv integrins that specific expressed in tumor vascular endothelium, and then is subjected to a proteolytic cleavage, exposing the CendR motif (RGDK/R) that binds to neuropilin-1 (NRP-1) and triggers extravasation and tissue penetration [28]. Co-administration of iRGD was more effective in delivering therapeutic agents into tumor parenchyma than conjugation [29]. This denied additional demands on chemical conjugation and greatly simplifies the path to clinical application, thereby providing a versatile way to enhance the anti-glioma delivery of currently investigated DDS. Considering that αv integrins and NRP-1 are both over-expressed on tumor vessels and glioma cells [30,31], we proposed that iRGD may provide a promising solution to overcome high interstitial fluid pressure and binding-site barrier and help in improving specific extravasation and penetration of active targeting nanoparticles into the glioblastoma.

In the present study, encapsulating paclitaxel (PTX) as the model drug, an active targeting DDS was constructed by conjugating MT1-AF7p to poly (ethyleneglycol)-poly (lactic acid) nanoparticles, and iRGD was co-administrated to enhance glioblastoma-specific drug accumulation and penetration. *In vitro* C6 glioma cell model and *in vivo* the orthotropic C6 glioma-bearing nude mice model were used to evaluate the glioblastoma targeting effect of MT1-NP and the extravasation and penetration improvement of iRGD.

2. Materials and methods

2.1. Materials

Methoxy poly (ethylene glycol) $_{3000}$-poly (lactic acid) $_{34,000}$ (MePEG-PLA) and maleimide-poly (ethylene glycol) $_{3400}$-poly (lactic acid) $_{34,000}$ (Male-PEG-PLA) were kindly provided by East China University of Science and Technology. MT1-AF7p (HWKHLHNTKTFLC) and iRGD (CRGDKGPDC) were synthesized by ChinaPeptides Co., Ltd (Shanghai, China). Paclitaxel was purchased from Xi'an Sanjiang Bio-Engineering Co. Ltd. (Xi'an, China) and Taxol® from Bristol-Myers Squibb Company. Annexin V-FITC Apoptosis Detection kit was purchased from Beyotime® Biotechnology Co. Ltd (Nantong, China), cell counting kit-8 (CCK-8) was provided by Dojindo (Kumamoto, Japan) and BCA protein assay kit by Pierce (Rockford, IL, USA). Alexa Fluor® 647 anti-mouse CD31 Antibody was obtained from Biolegend (San Diego, CA, USA). Hoechst 33258 and Coumarin-6 were obtained from Sigma–Aldrich (St. Louis, MO, USA), and 4,6-diamidino-2-phenylindole (DAPI) from Molecular Probes (Eugene, OR, USA). 1, 1′-dioctadecyl-3, 3, 3′, 3′-tetramethyl indotricarbocyanine Iodide (DiR) was purchased from Biotium (Hayward, CA). Dulbecco's modified Eagle's medium (high glucose) (DMEM), fetal bovine serum (FBS), Trypsine-EDTA (0.25%), penicillin-streptomycin and agarose were purchased from Gibco (Invitrogen, USA). All the other solvents were of analytical or chromatographic grade.

Male BALB/c nude mice (20 ± 2 g) were purchased from the BK Lab Animal Ltd (Shanghai, China) and maintained at 25 ± 1 °C with free access to food and water. All the animal experiments were carried out in accordance with guidelines evaluated and approved by the ethics committee of Fudan University (Shanghai, China).

2.2. Preparation of NP and MT1-NP

PEG-PLA nanoparticles (NP) were prepared via the emulsion/solvent evaporation technique as described elsewhere [32]. Briefly, 22.5 mg of MePEG-PLA and 2.5 mg of Maleimide-PEG-PLA were dissolved in 1 ml of dichloromethane, added into 2 ml of 1% sodium cholate and applied to ultrasonication for 30 s at 280 W on ice using probe sonicator (Ningbo Scientz Biotechnology Co. Ltd., China). Then the emulsion was diluted into 10 ml of 0.5% sodium cholate aqueous solution under magnetic stirring for 5 min before evaporating dichloromethane with a rotary evaporator (Shanghai Institute of Organic Chemistry, China). The formed NP was collected by centrifugation at 14,500 rpm using a TJ-25 centrifuge (Beckman Counter, USA) at 4 °C for 1 h and resuspended in 1 ml 0.01 M HEPES buffer (pH 7.0). Nanoparticles modified with MT1-AF7p (MT1-NP) were prepared via a maleimide-thiol coupling reaction at room temperature for 8 h. The products were then eluted with 0.01 M HEPES buffer (pH 7.0) through a 1.5 × 20 cm sepharose CL-4B column to remove the unconjugated peptide.

PTX-, coumarin-6- and DiR-loaded nanoparticles were prepared with the same procedure except 0.5 mg PTX, 25 μg coumarin-6 or 0.25 mg DiR were dissolved in the dichloromethane solution.

2.3. Characterization of nanoparticles

2.3.1Particle size distribution, zeta potential and morphology

Particle size and zeta potential of the nanoparticles were determined with a dynamic light scattering detector (Zetasizer, Nano-ZS, Malvern, UK). The morphological examination of nanoparticles was performed by transmission electron microscope (TEM) (H-600, Hitachi, Japan) following negative staining with 2% sodium phosphotungstate solution.

2.3.2Encapsulation efficiency (EE) and loading capacity (LC)

The encapsulation efficiency (EE) and loading capacity (LC) of PTX-loaded PEG-PLA nanoparticles (NP-PTX) and PTX-loaded PEG-PLA nanoparticles modified with MT1-AF7p (MT1-NP-PTX) were investigated as previously described [33].

The EE% and LC% were calculated as indicated below:

$$EE(\%) = \frac{\text{Amount of PTX in the nanoparticles}}{\text{Total amount of PTX added}} \times 100\%$$

$$LC(\%) = \frac{\text{Amount of PTX in nanoparticles}}{\text{nanoparticles weight}} \times 100\%$$

2.3.3In vitro PTX release

The *in vitro* release behaviors of PTX from the nanoparticles were investigated by dialysis method [34]. PTX-loaded nanoparticles were purified via a 1.5 × 20 cm sepharose CL-4B column to remove unentrapped PTX. A volume of 1 ml PTX formulation (containing 80 μg PTX) was pipetted into a dialysis bag (MWCO = 8000 Da) and dialyzed against 40 ml of PBS (pH 7.4) with 0.5% Tween-80

at 37 °C with shaking at 120 rpm/min. At predetermined time points, 200 μl of sample was withdrawn and the concentration of PTX was analyzed by HPLC as described previously [33].

2.3.4. MT1-AF7p density on nanoparticle surface

MT1-AF7p level on the nanoparticle surface was determined via a BCA Protein Assay using unmodified nanoparticles at the same concentration as the blank [35]. NP and MT1-NP resuspended in PBS (pH 7.4) were added into a 96-well plate (20 μl/well) and incubated with 160 μl of BCA Protein Assay Reagent at 37 °C for 1 h, respectively. After that, the absorption was measured via a microplate reader (Thermo Multiskan MK3, USA) at 562 nm.

MT1-AF7p conjugation efficiency (CE%) was calculated to determine the percentage of MT1-AF7p peptide conjugated to the nanoparticles surface with the formula as follows:

$$\mathrm{CE}(\%) = \frac{\text{Amount of MT1} - \text{AF7p on the surface of nanoparticle}}{\text{Total amount of MT1} - \text{AF7p added}} \times 100\%$$

MT1-AF7p peptide surface density (S) was calculated by dividing the number of MT1-AF7p molecules by the calculated average number (n) of nanoparticles with the formula: $n = 6 * m/(\pi * D^3 * \rho)$, in which m is the nanoparticle weight, D is the number-based mean nanoparticle diameter, and ρ is the nanoparticle weight per volume unit (density), estimated to be 1.1 g/cm^3 [36].

2.4. Cellular association of coumarin-6-labeled nanoparticles in C6 cells

2.4.1Cell culture

C6 glioma cells were cultured in DMEM supplemented with 10% FBS, penicillin (100 U/ml) and streptomycin (100 μg/ml) under standardized conditions (95% relative humidity, 5% CO_2, 37 °C).

2.4.2Fluorescent microscopy analysis of nanoparticles association in C6 cells

Qualitative analysis of cellular association of NP and MT1-NP was performed via fluorescent microscopy, using coumarin-6 as the fluorescent probe. C6 cells were seeded into 24-well plates at the density of 4×10^4 cells per well, and allowed to grow for 24 h. Then the cells were incubated with the nanoparticles in serum-free DMEM for 1 h at the concentrations ranging from 50 to 400 μg/ml at 37 °C. At the end of the experiment, the cells were washed three times with PBS, fixed with 4% formaldehyde for 15 min and then subjected to fluorescent microscopy analysis (Leica DMI4000 B, Germany).

2.4.3Quantitative analysis of nanoparticles association in C6 cells

Quantitative analysis of cellular association of coumarin-6-loaded NP and MT1-NP was evaluated with a High Content Cell Analysis System (HCS). Briefly, C6 cells were seeded in 96-well plates at the density of 5000 cells/well. After 24 h incubation, the cells were incubated with the nanoparticles in DMEM for 1 h at the concentrations ranging from 50 to 400 μg/ml, at 4 °C and 37 °C, respectively. In order to study the effects of incubation time on nanoparticle association, C6 cells were incubated with 200 μg/ml nanoparticles for 30 min, 1, 2 and 4 h at 37 °C, respectively. Thereafter, the cells were washed with PBS and fixed with 4% formaldehyde solution for 15 min and stained with 2 μg/ml Hochest 33258 at room temperature for 10 min away from light. After that, the cells was washed for three times and detected under a KineticScan® HCS Reader (version 3.1, Cellomics Inc., Pittsburgh, PA, USA).

2.5. Mechanism of cellular internalization of MT1-NP

In order to elucidate the mechanism of cellular internalization of MT1-NP in C6 cells, endocytosis inhibition experiments were performed in the presence of various endocytosis inhibitors. C6 cells were seeded in a 96-well plate at the density of 5000 cells/well and cultured for 24 h. After checking the confluency and morphology, chlorpromazine (10 μg/ml), colchicines (4 μg/ml), Cytochalasin D (cyto-D, 10 μg/ml), BFA (5 μg/ml), filipin (5 μg/ml), NaN_3 (10 mM) plus deoxyglucose (50 mM), methyl-β-cyclodextrin (M-β-CD, 2.5 mM), monensin (200 nM), nocodazole (20 μM) or MT1-AF7p peptide (200 μg/ml) was added into each well and incubated for 1 h. After that, the cells were incubated with coumarin-6-labeled MT1-NP (200 μg/ml) for 1 h at 37 °C. Quantitative analysis of the cellular association of nanoparticles following the inhibitor treatments was performed as abovementioned and compared with that of the non-inhibited control.

2.6. Anti-proliferation assay

C6 cells in the logarithmic growth phase were seeded into 96-well plates at the density of 5000 cells/well and cultured at 37 °C in a humidified atmosphere with 5% CO_2 for 24 h. Thereafter, the medium was removed, and the cells were exposed to serum-free medium containing PTX formulations, including Taxol®, NP-PTX and MT1-NP-PTX with various concentrations. After 72 h incubation, cell viability was evaluated via a Cell Counting Kit-8 (CCK-8) assay according to the manufacturer's instruction. The IC_{50} values were calculated by nonlinear regression analysis using GraphPad Prism® 5.0 software.

2.7. Cell apoptosis assay

C6 cells were seeded in 6-well plates at the density of 5×10^5 cells per well, cultured for 24 h, and then incubated for 24 h with Taxol®, NP-PTX and MT1-NP-PTX, respectively, at the PTX concentration of 100 ng/ml using drug-free culture medium as the negative control. After that, the cells were fixed with 4% paraformaldehyde for 15 min, stained with 10 μg/ml Hoechst 33528 at room temperature for 15 min, and washed twice with ice-cold PBS. Finally, the nuclear morphology was checked using a fluorescent microscope (Leica DMI4000 B, Germany).

For quantitative analysis, the cells treated with the PTX formulations (100 ng/ml) were stained with an Annexin V-FITC Apoptosis Detection kit according to the manufacture's instructions and analyzed under a flow cytometer (FACSCalibur, BD, USA).

2.8. Penetration in tumor spheroid

Three-dimensional (3 D) multicellular tumor spheroids of C6 cells were established to mimick the solid tumors *in vivo* using a lipid overlay system as reported previously [37]. Firstly, the cells were seeded in 48-well plates which was pre-coated with 150 μl of a 2% low-melting-temperature agarose at a density of 2×10^3 cells/well. Subsequently, the culture plates were allowed to agitate gently for 5 min and cultured at 37 °C for 7 days. After that, those spheroids with temperate size and tight cell interaction were treated with 400 μg/ml coumarin-6-loaded NP or MT1-NP for 4 h, rinsed three times with ice-cold PBS and fixed in 4% paraformaldehyde for 30 min before subjection to laser scanning confocal microscopy analysis (LSM510, Leica, Germany).

2.9. Inhibition of tumor spheroid growth

C6 glioma spheroids were prepared as described above. Seven days after seeding, the spheroids were incubated with 200 μl of serum-free DMEM containing Taxol®, NP-PTX and MT1-NP-PTX, respectively at the PTX concentration of 0.5 μg/ml with those treated with drug-free DMEM as the blank controls. Growth inhibition following drug treatment was evaluated by measuring the size of the C6 glioma spheroids using an inverted phase microscope fitted with an ocular micrometer on days 0, 1, 3, 5 and 7. Spheroid volume was calculated as previously mentioned by using the following formula: $V = (\pi \times d_{max} \times d_{min})/6$ where d_{max} is the maximum and d_{min} the minimum diameter of the spheroid. The change in tumor spheroid volume was reflected by the formula: ratio% $= (V_{dayi}/V_{day0}) \times 100$, where V_{dayi} is the volume of the tumor spheroid on the ith day (day 1, 3, 5, 7) after drug application, and V_{day0} is the volume of tumor spheroid prior to treatment [38].

2.10. In vivo imaging

Nude mice bearing orthotropic C6 glioma was prepared as reported previously [33]. Briefly, 5.0×10^5 C6 cells suspended in 5 μl PBS were implanted into the right striatum (1.8 mm lateral to the bregma at 3 mm depth) of male BALB/c nude mice using a stereotactic fixation device with a mouse adapter. Fourteen days after implantation, the mice were divided into four groups. DiR-loaded NP and MT1-NP were intravenous injected into mice at the dose of 1 mg/kg DiR, and the co-adminstration peptide iRGD was given at the dose of 4 μmol/kg 5 min after the NPs injection. The fluorescent distribution was captured under a CRi *in vivo* imaging system (CRi, MA, USA) at 2, 6, 12 and 24 h following administration. After that, the mice were sacrificed with tumor-bearing brains and other major organs, including hearts, livers, spleens, lungs and kidneys collected and imaged.

2.11. In vivo glioma distribution

Mice bearing intracranial C6 glioma were established as described above and housed at standard condition for 2 weeks. After that, the mice were divided into four groups and injected intravenously with coumarin-6-loaded NP, coumarin-6-loaded NP + iRGD, coumarin-6-loaded MT1-NP, coumarin-6-loaded MT1-NP + iRGD, respectively, at the dose of iRGD 4 μmol/kg and an equal dose of coumarin-6. Three hours later, the mice were anesthetized and heart perfused with saline and 4% paraformaldehyde with the brains harvested. The brains were the fixed in 4% paraformaldehyde, dehydrated in 15% sucrose and 30% sucrose sequentially before OCT (Sakura, Torrance, CA, USA) embedding and frozen section (10 μm thickness). For immunostaining, the slides were firstly blocked with 20% goat serum for 1 h at room temperature, and then incubated with Alexa Fluor® 647 anti-mouse CD31 antibody (1 × 100 dilution) overnight at 4 °C. Finally, the slides were subjected to DAPI for nuclear counterstain and visualized under a Zeiss LSM 510 confocal microscope.

2.12. Anti-glioma activity

To evaluate the anti-glioma activity, BALB/c nude mice (20 ± 2 g) bearing intracranial C6 glioma were established as described above and randomly divided into six groups. At 7, 10, 13, 16, 19 and 22 days after implantation, the mice received an intravenous injection of physiological saline, Taxol®, NP-PTX, NP-PTX with

co-administration of iRGD peptide, MT1-NP-PTX, MT1-NP-PTX with co-administration of iRGD peptide, respectively, at the dose of PTX 5 mg/kg and iRGD 4 μmol/kg. The survival of the animals was recorded, presented by Kaplan–Meier plots and analyzed with log-rank test.

2.13. Statistical analysis

All the data were presented as mean ± SD unless otherwise indicated. Comparison among the different groups was performed by one-way ANOVA followed by Bonferroni tests. A value of $p < 0.05$ was considered significant.

3. Results

3.1. Characterization of NP and MT1-NP

Representative TEM photographs illustrated that NP-PTX and MT1-NP-PTX were both generally spherical (Fig. 1A, B). Dynamic light scattering analysis showed that NP-PTX exhibited an average diameter of about 115.67 ± 9.83 nm, which was slightly increased to around 131.33 ± 4.94 nm after MT1-AF7p conjugation, with quite narrow size distribution (Table 1). The zeta potential of NP-PTX (−36.67 ± 2.72 mV) was slightly lower than that of MT1-NP-PTX (−31.43 ± 3.78 mV).

The MT1-AF7p peptide conjugation efficiency was 27.2 ± 3.1% and the MT1-AF7p peptide density on the nanoparticle surface was 317 ± 23 under our experiment conditions (weight ratio of Male-PEG-PLA to MPEG-PLA 1:9, molar ratio of mal-PEG-PLA to MT1-AF7p peptide 1:2 and incubation time for conjugation reaction 8 h).

The EE of the optimized NP-PTX and MT1-NP-PTX was 42.60 ± 3.63% and 41.03 ± 3.03%, respectively, with the LC 1.31 ± 0.14% and 1.21 ± 0.05%, respectively.

Table 1
Physical characterization of NP-PTX and MT1-NP-PTX (Data represent mean ± SD, $n = 3$).

Nanoparticles	Mean size (mean ± SD, nm)	Polydispersity index (P.I.)	Zeta potential (mV)
NP-PTX	115.67 ± 9.83	0.15 ± 0.02	−36.67 ± 2.72
MT1-NP-PTX	131.33 ± 4.94	0.20 ± 0.03	−31.43 ± 3.78

In vitro release experiment showed that NP-PTX and MT1-NP-PTX displayed a similar sustained-release profile in which the total PTX release from nanoparticles were about 52% in the first 24 h and 80% in 96 h. In contrast, in the case of Taxol®, complete release was obtained in 12 h.

3.2. Cellular association in C6 glioma cells

Fluorescent microscopy analysis showed that after 1 h exposure to coumarin-6-loaded MT1-NP and NP, the cellular associated fluorescent signal in C6 cells correlated with the increase of nanoparticle concentration (Fig. 2A). A higher accumulation of MT1-NP in the cells was observed compared with that of NP.

Quantitative analysis confirmed the concentration-dependent cellular association of NP and MT1-NP in C6 cells (Fig. 2B). Besides, the association of both coumarin-6-loaded NP and MT1-NP under 37 °C was much greater than that under 4 °C, suggesting that the internalization of both nanoparticles was temperature-dependent. Furthermore, the association of NP and MT1-NP by C6 cells was dependent on the incubation time within 4 h (Fig. 2C).

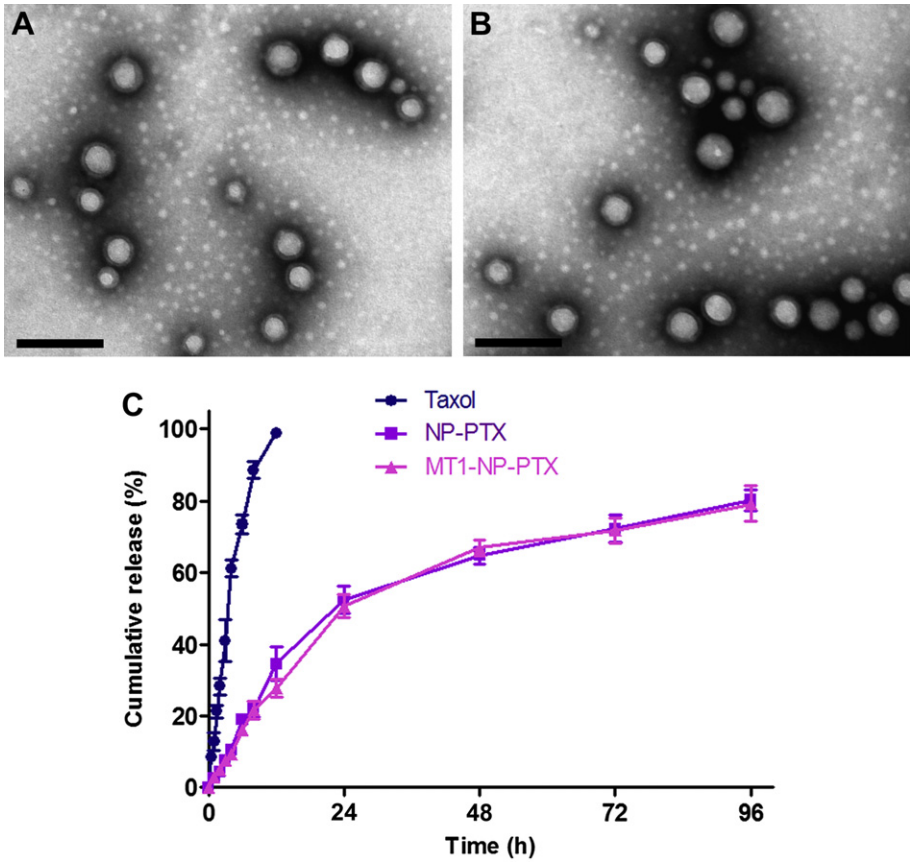

Fig. 1. Transmission electron micrograph of NP-PTX (A) and MT1-NP-PTX (B). PTX release profiles from Taxol®, NP-PTX and MT1-NP-PTX in PBS (pH 7.4) with 0.5% Tween-80 at 37 °C (C). The bar is 200 nm.

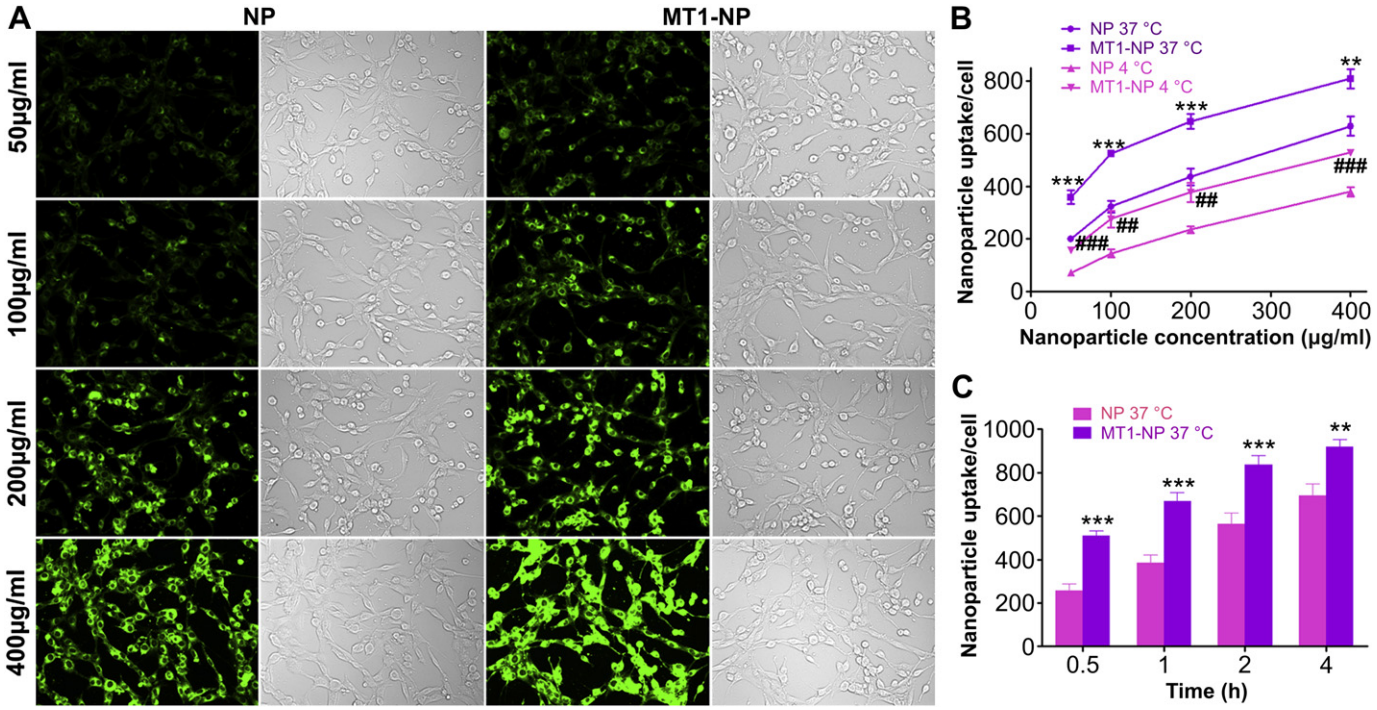

Fig. 2. (A) In vitro cellular association coumarin-6-labeled NP and MT1-NP after 1 h incubation at 37 °C at the concentrations of 50 μg/ml, 100 μg/ml, 200 μg/ml, 400 μg/ml, respectively. Original magnification: 20×. (B) Quantitative cellular association of NP and MT1-NP in C6 cells after 1 h incubation with different concentrations of coumarin-6-labeled nanoparticles (from 50 μg/ml to 400 μg/ml) at 37 °C and 4 °C. (C) Quantitative cellular association of NP and MT1-NP in C6 cells after incubation for 0.5 h–4 h at the NPs concentration of 200 μg/ml. Data presented as mean ± SD ($n = 3$). $^{*}p < 0.05$, $^{**}p < 0.01$, $^{***}p < 0.001$ significantly higher than the cellular association of unmodified NP at 37 °C, and #$p < 0.05$, ##$p < 0.01$, ###$p < 0.001$ significantly higher than the cellular association of unmodified NP at 4 °C.

3.3. Mechanism of cellular internalization of MT1-NP

Endocytosis inhibition experiment showed that the cellular association of MT1-NP was significantly inhibited by actin-disrupting agent – cyto-D and Golgi apparatus destroyer – BFA ($p < 0.001$, $p < 0.01$, respectively) (Fig. 3). Besides, energy-depletion agent – NaN_3 and lipid raft inhibitor – M-β-CD significantly reduced the cellular internalization of MT1-NP ($p < 0.001$, $p < 0.05$, respectively). Furthermore, pre-added MT1-AF7p peptide also significantly inhibited the cellular association of MT1-NP ($p < 0.01$).

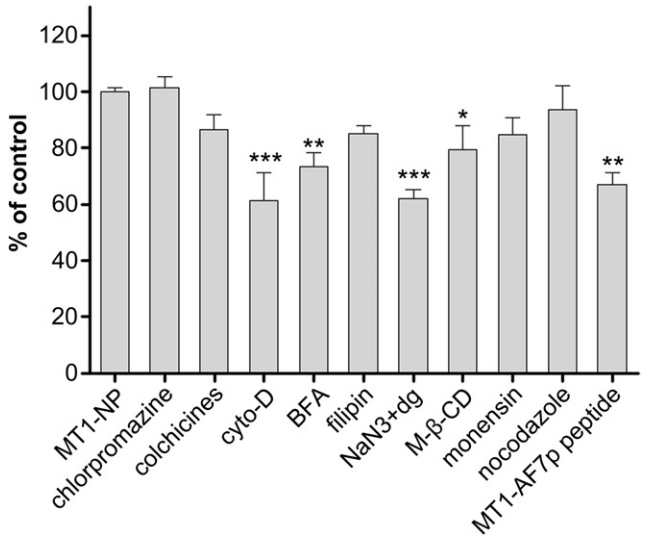

Fig. 3. Effects of inhibitors on the cellular internalization of coumarin-6-labeled MT1-NP in C6 glioma cells. Fluorescence intensity of coumarin-6 in the non-inhibited cells, representing the maximum internalized amount of coumarin-6-labeled MT1-NP, was taken as control. $^{*}p < 0.05$, $^{**}p < 0.01$, $^{***}p < 0.001$ compared with control ($n = 3$).

3.4. Anti-proliferation assay

The anti-proliferation activity of Taxol®, NP-PTX and MT1-NP-PTX on C6 glioma cells was evaluated via a CCK-8 assay (Fig. 4). The IC_{50} were 87.11 nM for Taxol®, 76.34 nM for NP-PTX and 31.03 nM for MT1-NP-PTX, respectively. The IC_{50} value of MT1-NP-PTX was 2.81 and 2.47 folds lower than that of Taxol® and NP-PTX, respectively.

3.5. Cell apoptosis assay

The nuclei of untreated C6 cells were spherical and integrated (Fig. 5A), but became severely fragmented after treated with the PTX formulations for 24 h (Fig. 5C, E, G). Compared with Taxol® and NP-PTX, MT1-NP-PTX induced more severe fragmentation of the cell nuclei.

For quantitative analysis, Annexin V-FITC Apoptosis Detection kit was used to stain the cells and the percentage of cell apoptosis was determined via a flow cytometer (Fig. 5B, D, F, H). The percentage of early and late apoptosis of those cells treated with Taxol® was 7.31 ± 1.18% and 4.94 ± 0.82%, respectively, while those with NP-PTX was 10.74 ± 2.22% and 8.48 ± 0.88%, respectively. In contrast, the percentage of early and late apoptosis of the cells treated with MT1-NP-PTX was 15.51 ± 1.13% and 12.08 ± 1.49%, respectively, the highest among the three treatments.

3.6. Penetration in tumor spheroid

In vitro avascular C6 glioma spheroid was used for evaluating the tumor penetration activity of MT1-NP. As showed by confocal

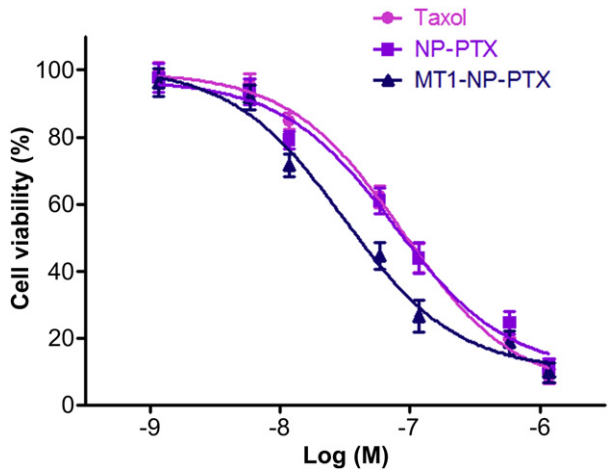

Fig. 4. In vitro cytotoxicity of Taxol®, NP-PTX and MT1-NP-PTX on C6 glioma cells. The C6 cells were plated at 5000 cells per well in the 96-well plate and cultured in growth medium for 24 h prior to exposure to Taxol®, NP-PTX and MT1-NP-PTX for 72 h at 37 °C.

microscopy analysis (Fig. 6B, C), surface conjugation with MT1-AF7p peptide led to a higher association of nanoparticles with the C6 glioma spheroid. What's more, compared with NP, MT1-NP penetrated deeper into the tumor spheroids.

3.7. Inhibition of tumor spheroid growth

Inhibition of tumor spheroid growth was evaluated following the treatment with Taxol®, NP-PTX and MT1-NP-PTX, respectively. C6 glioma spheroids treated with serum-free DMEM grew fast and became more compact, whereas those treated with Taxol®, NP-PTX and MT1-NP-PTX stopped to grow and even became smaller (Fig. 7A). After the treatment with MT1-NP-PTX, the tumor spheroids were distorted and shrunken, and almost lost their three-dimensional structure. After treated for 7 days, the C6 glioma spheroid volume ratios were 288.7 ± 24.5% for serum-free DMEM, 108.3 ± 6.5% for Taxol®, 76.7 ± 10.9% for NP-PTX and 31.0 ± 5.6% for MT1-NP-PTX, respectively (Fig. 7B).

3.8. In vivo imaging

The fluorescence signal of MT1-NP detected in the tumor-bearing brain was much stronger than that of NP, and slightly higher than that of NP co-administrated with iRGD (Fig. 8A, B, C). Co-administration with iRGD apparently increased the accumulation of DiR in the glioma-bearing brain of nude mice treated NP or MT1-NP, respectively (Fig. 8B, D). MT1-NP co-administrated with iRGD demonstrated the highest fluorescence intensity at the tumor site at all the time points post-injection (Fig. 8D). Semi-quantitative analysis of region of interest (ROI) revealed that the intensity of MT1-NP co-administrated with iRGD in the glioma was 4.86, 2.01, 1.90-fold over that of NP, NP co-administrated with iRGD and MT1-NP, respectively (Fig. 8E).

3.9. In vivo glioma distribution

When injected alone, NP was found mainly entrapped in the tumor blood vessles (Fig. 9). Whereas, after co-administrated with iRGD, an appropriate amount of NP was observed to extravasate and accumulate in the glioma. MT1-NP displayed a glioma distribution profile comparable to that of NP co-administrated with iRGD. MT1-NP co-administrated with iRGD showed a significantly wider and higher distribution than the other three formulations 3 h after i.v. administration (Fig. 9).

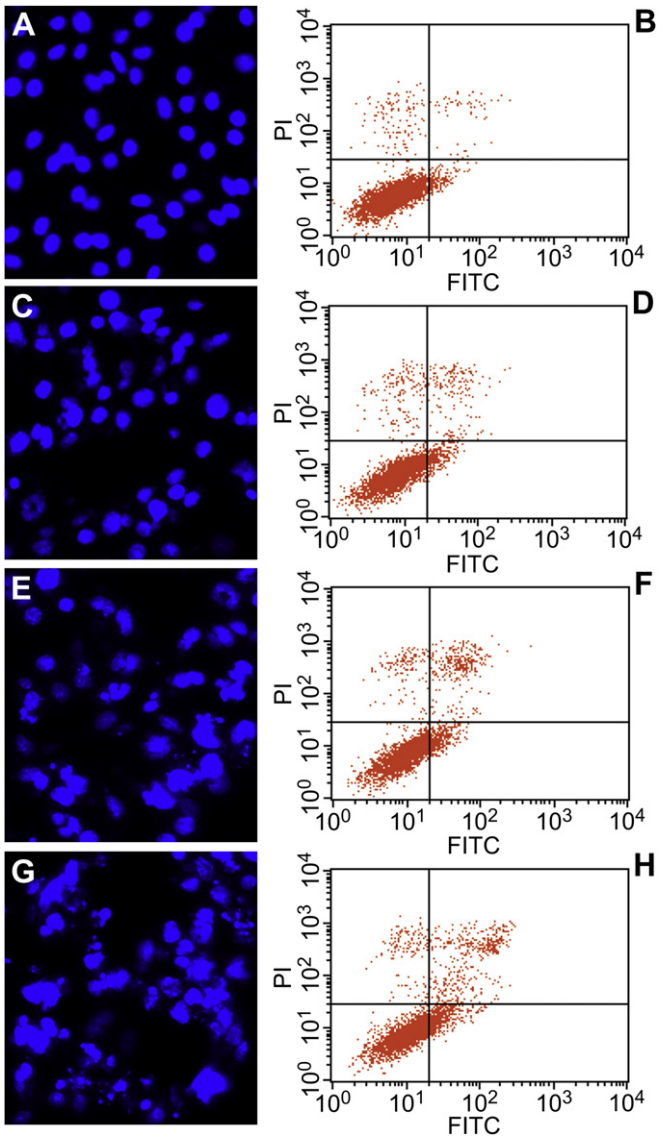

Fig. 5. Induction of apoptosis on C6 glioma cells by Taxol® (C, D), NP-PTX (E, F) and MT1-NP-PTX (G, H) after incubation for 24 h at equivalent PTX concentration (100 ng/ml). Normal C6 glioma cells without any treatment served as the control (A, B). Fluorescence micrographs of C6 glioma cell nuclei labeled by Hoechst 33258 (A, C, E and G). Flow cytometry used staining of Annexin V-FITC and PI (B, D, F and H). Original magnification: ×20.

3.10. Anti-glioma activity

The anti-glioma effect was evaluated in nude mice bearing intracranial C6 glioma. As shown in Fig. 10, the median survival of mice treated with MT1-NP-PTX + iRGD (60 days) was significantly longer than those of mice treated with physiological saline (21 days, $p < 0.001$), Taxol® (24 days, $p < 0.001$), NP-PTX (32 days, $p < 0.001$), NP-PTX + iRGD (40 days, $p < 0.01$) and MT1-NP-PTX (48 days, $p < 0.05$) (Table 2). Additionally, MT1-NP-PTX significantly prolonged animal survival when compared with NP-PTX with co-administration of iRGD peptide ($p < 0.05$).

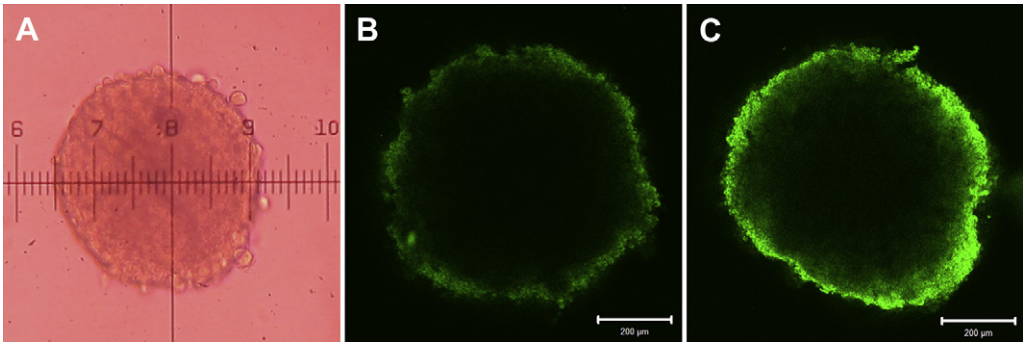

Fig. 6. The C6 tumor spheroid at day 7 after cells seeded, images were acquired at 10×. Confocal microscope images of C6 tumor spheroids incubated with (B) coumarin-6-labeled NP and (C) coumarin-6-labeled MT1-NP for 4 h. The bar is 200 μm.

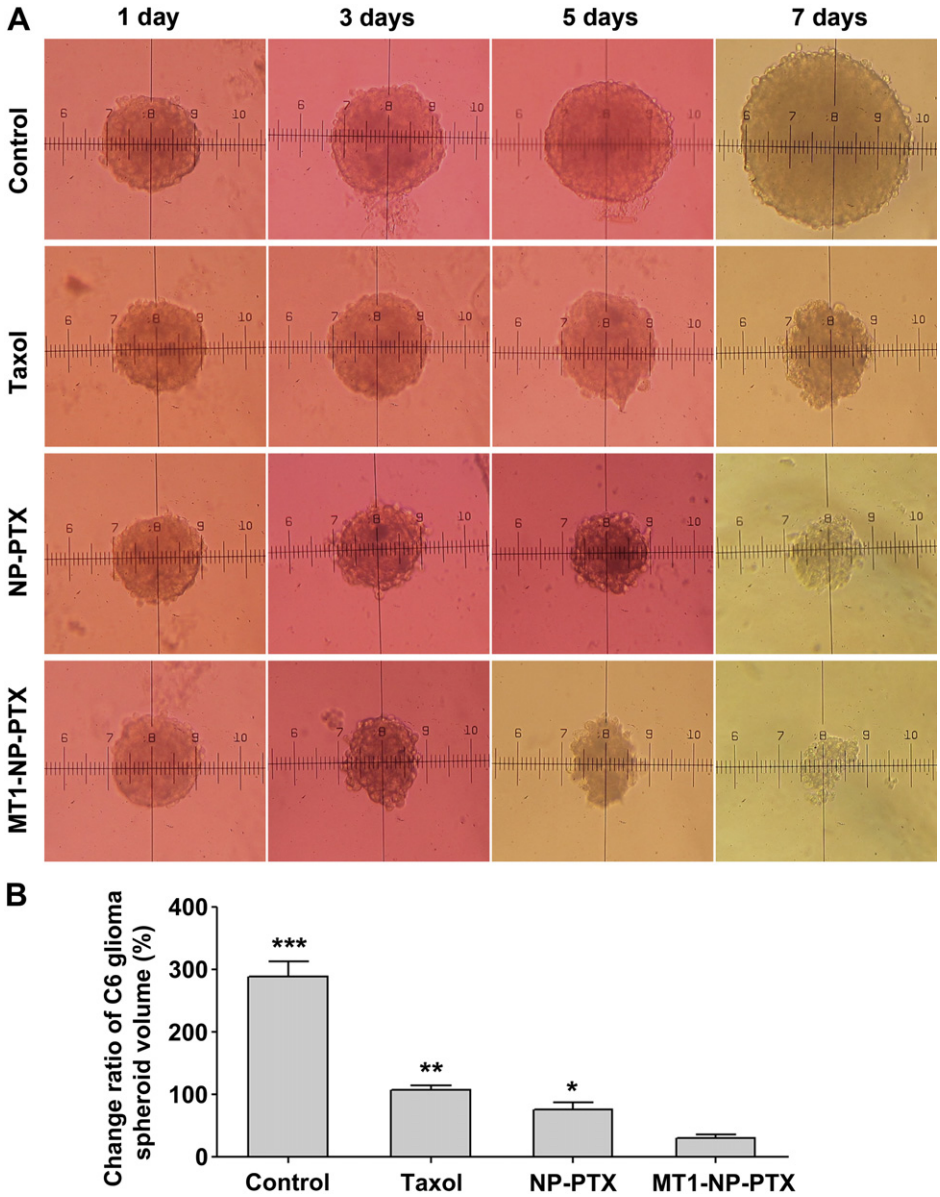

Fig. 7. (A) Inhibition of tumor spheroid growth was evaluated following the treatment with Taxol®, NP-PTX and MT1-NP-PTX, respectively, at the PTX concentration of 0.5 μg/ml with those treated with drug-free DMEM as the blank control. The images were taken on day 1, 3, 5, 7 under invert microscope fitted with an ocular micrometer. (B) Change of glioma spheroids volume (%) after the treatment of various PTX formulations (Taxol®, NP-PTX and MT1-NP-PTX) and drug-free DMEM (Control) ($n = 3$). $^{*}p < 0.05$, $^{**}p < 0.01$, $^{***}p < 0.001$ statistically significant difference with respect to MT1-NP-PTX. All error bars reflect SD.

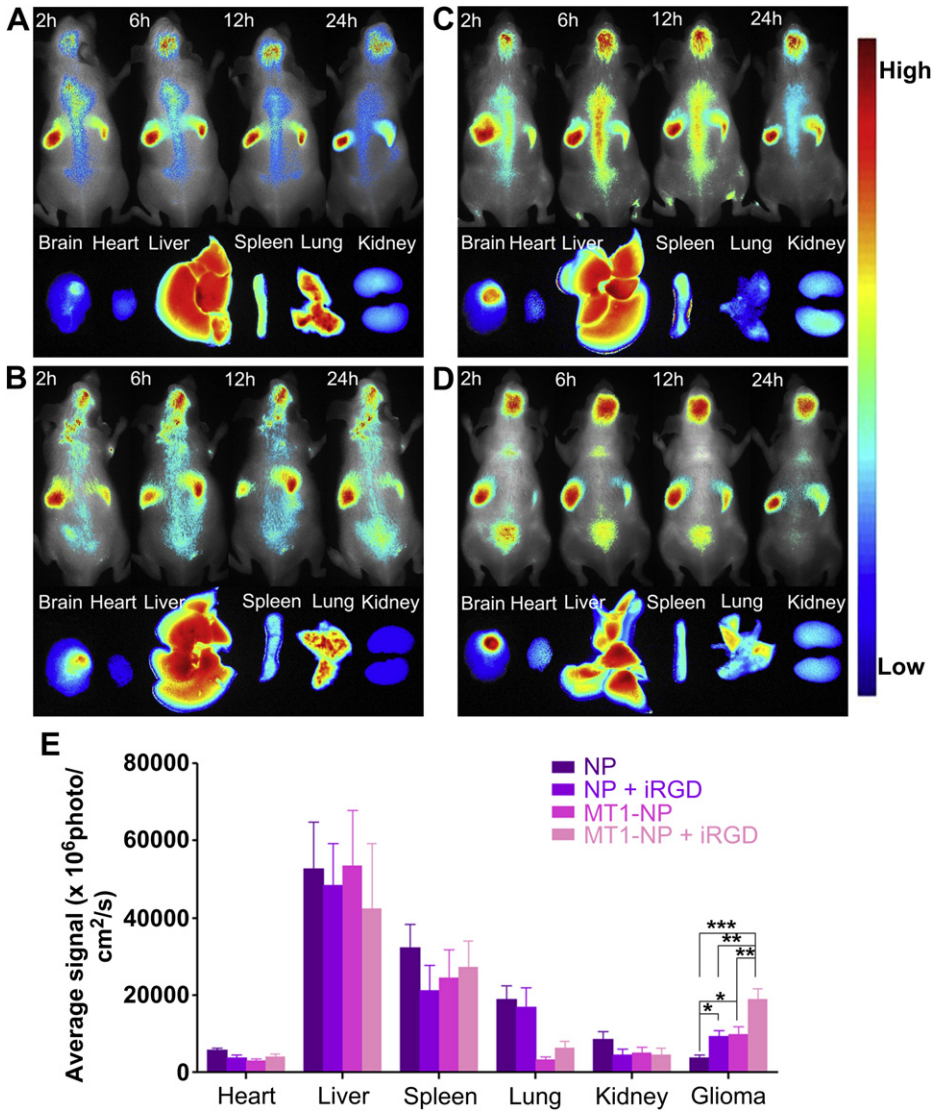

Fig. 8. In vivo fluorescence imaging of intracranial C6 glioma-bearing nude mice and the dissected organs after intravenous injection with DiR-labeled NP (A), NP in combination with iRGD (B), MT1-NP (C) and MT1-NP in combination with iRGD (D). Semi-quantitative analysis of the fluorescent intensity of the formulations in different organs and glioma (E). The data presented mean ± SD ($n = 3$), $^{*}p < 0.05$; $^{**}p < 0.01$; $^{***}p < 0.001$.

4. Discussion

Glioblastoma represents the second cause of cancer death in adults less than 35 years of age [39]. More than 70% of patients with glioblastoma succumb to the disease in two years, and less than 10% survive 5 years post diagnosis [40]. Improvements in chemotherapy against glioblastomas have not been translated into a meaningful improvement in patient outcome due to the therapeutics' low permeability across the BTB and poor penetration into the glioma parenchyma. The growing awareness of this fact underscores the importance of pursuing more rational drug delivery strategies.

In this contribution, we proposed MT1-AF7p-conjugated PEG-PLA nanoparticles (MT1-NP) as a dual-targeting DDS for glioblastoma treatment as the target of MT1-AF7p peptide – MT1-MMP over-expressed on both BTB and glioma cells. PLA was chosen as the drug carrier as it possesses the advantages over other polymers including physical stability, sustained drug release and FDA approved safety for human use [41]. In order to further increase extravasation and penetration of the nanoparticles into the glioma parenchyma, MT1-NP was co-administrated with iRGD peptide, which mediated tumor homing via binding to αv integrins that specific expressed in tumor endothelium and followed by a proteolytic cleavage, exposing the CendR motif that binded to NRP-1 and triggered tissue penetration [29]. Although other CendR peptides such as tLyp-1 could also be co-administrated for improving extravasation of nanoparticles, tumor targeting efficiency can not be guaranteed as the CendR receptors – neuropilins are ubiquitously expressed *in vivo*, albeit that the expression in tumor tends to be higher [42]. The prior recognization by integrins confers on iRGD tumor-specific activity, making iRGD distinguished from other CendR peptides.

Particle size is one crucial determinant of nanoparticle accumulation and penetration in tumor. In our study, the average diameter of NP-PTX was increased from 115.67 ± 9.83 nm to 131.33 ± 4.94 nm following MT1-AF7p modification. As particles from 5 to 250 nm, in general, exhibit higher transport efficiency [43], the nanoparticles obtained here met such requirement. In terms of drug encapsulation, a slightly lower EE was achieved by MT1-NP-PTX than NP-PTX, most likely due to the drug release during the peptide conjugation. Furthermore, *in vitro* release

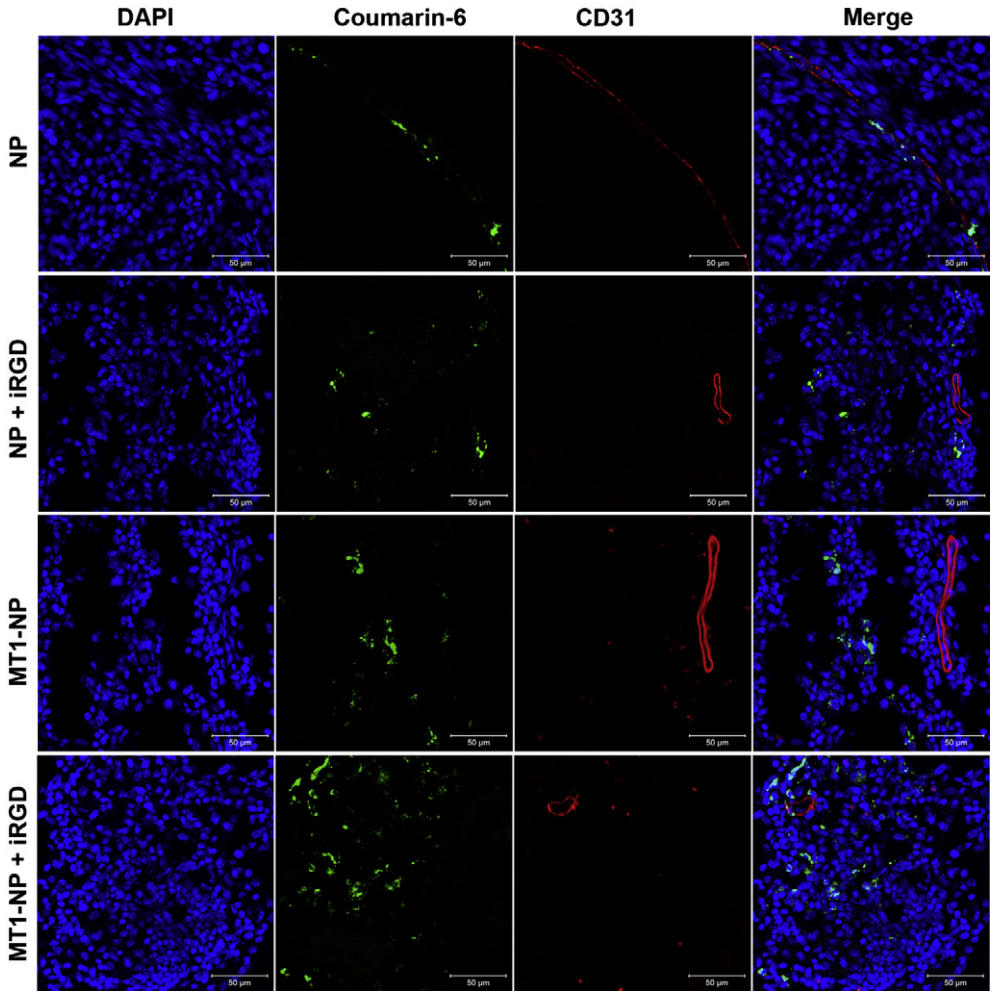

Fig. 9. Distribution of the coumarin-6-labeled NP, NP co-administrated with iRGD, MT1-NP, MT1-NP co-administrated with iRGD in the brain of nude mice bearing intracranial C6 glioma 3 h after i.v. administration. Frozen sections were examined under a confocal microscope. Blood vessels were visualized with anti-CD31 (red), nuclei were stained with DAPI (blue), while green was represented the NPs. Bars represent 50 μm. (For interpretation of the references to color in this figure legend, the reader is referred to the web version of this article.)

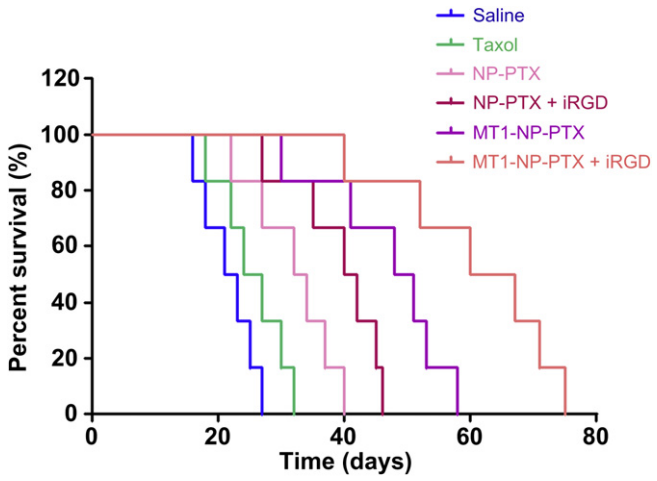

Fig. 10. Kaplan–Meier survival curves of intracranial C6 glioma-bearing mice treated with Taxol®, NP-PTX, NP-PTX in combination with iRGD, MT1-NP-PTX, MT1-NP-PTX in combination with iRGD (PTX dose 5 mg/kg, iRGD dose 4 μmol/kg) and saline, respectively, at day 7, 10, 13, 16, 19 and 22 post implantation ($n = 6$).

results showed that the decoration of MT1-AF7p peptide did not change the release profile of the nanoparticles.

Cellular association of PEG-PLA nanoparticles in C6 cells was enhanced following the MT1-AF7p functionalization (Fig. 2A). As shown by HCS analysis, cellular association of nanoparticles was time-, temperature- and concentration- dependant (Fig. 2B, C), suggesting that the cellular internalization of MT1-NP was an active endocytosis process.

Understanding the internalization mechanism of nanoparticles is fundamental to their application as delivery vectors. Several mechanisms for cellular entry of nanoparticles range from direct cell penetration to clathrin/caveolin-mediated endocytosis and macropinocytosis. To clearly identify the pathway utilized by MT1-NP for their internalization into C6 cells, cellular association of the nanoparticles were performed in the presence of various endocytosis inhibitors [44,45]. It was found that cellular association of MT1-NP was significantly inhibited by actin-disrupting agent – cyto-D, energy-depletion agent – NaN_3, lipid raft inhibitor – M-β-CD, and Golgi apparatus destroyer – BFA (Fig. 3). As M-β-CD is regularly used to determine whether endocytosis is dependent on the integrity of lipid rafs [46] while cyto-D is mainly used to evaluate the contribution of macropinocytosis to endocytosis [47], therefore, our results suggested that in C6 cells the cellular internalization pathways utilized by MT1-NP included both energy-

Table 2
In vivo effects of PTX formulations on intracranial C6 glioma mice model ($n = 6$).

Groups	Mean survival time (days)	Median (days)	Compare with				
			Saline	Taxol®	NP-PTX	NP-PTX + iRGD	MT1-NP-PTX
Saline	21.7 ± 1.7	21	–	–	–	–	–
Taxol®	25.5 ± 2.1	24	$p > 0.05$	–	–	–	–
NP-PTX	32.0 ± 2.7	32	**	*	–	–	–
NP-PTX + iRGD	39.2 ± 2.9	40	***	**	*	–	–
MT1-NP-PTX	46.8 ± 3.1	48	***	**	**	*	–
MT1-NP-PTX + iRGD	60.8 ± 5.3	60	***	***	***	**	*

*$p < 0.05$, **$p < 0.01$, ***$p < 0.001$ of log-rank analysis.

dependent macropinocytosis and lipid raft-mediated endocytosis, with Golgi apparatus involved in the intracellular transport. Furthermore, the internalization of MT1-NP was inhibited by MT1-AF7p peptide, suggesting that the improved C6 cellular association was mainly contributed by MT1-AF7p conjugation.

In vitro cytotoxicity of PTX to C6 glioma cells was effectively enhanced following its encapsulation in MT1-NP. The results from the CCK-8 assay (Fig. 4) indicated that MT1-NP-PTX evidently decreased the IC_{50} value. Flow cytometry analysis of cell apoptosis (Fig. 5H) also demonstrated that MT1-NP-PTX increased the induction of both early and late apoptosis in C6 glioma cells. The improved anti-tumor activity of MT1-PTX-NP was believed to be attributed to the MT1-AF7p peptide, which facilitated the internalization of the formulation into the C6 glioma cells.

To evaluate the glioma-targeting efficiency of MT1-AF7p peptide co-administrated with iRGD, *in vivo* imaging experiment was performed in nude mice bearing intracranial C6 glioma using DiR, a near-infrared fluorescent dye, as an indicator [33]. Accumulation of MT1-NP in the intracranial tumor site was much higher than that of NP (Fig. 8A, C, E), suggesting that a good glioma-targeting effect could be achieved by MT1-NP. Co-administration with iRGD resulted in a much higher accumulation of nanoparticles at the tumor site, indicating that iRGD could effectively and specifically improve the delivery of nanoparticles to the tumor foci (Fig. 8B, D, E).

To evaluate the extravasation and penetration efficiency of the developed drug delivery strategy, *in vivo* glioma distribution was performed. It was found that NP was mainly entrapped in the tumor blood vessels, supporting the notion that with the development of glioblasoma, BBB becomes impaired but BTB remains a major obstacle to the access of nanoparticles to the tumor site. An appropriate amount of MT1-NP was found in the glioma parenchyma, indicating the BTB/glioma cells dual-targeting DDS might facilitate extravascular transport of nanoparticles and enhance penetration of nanoparticles within the tumor via an MT1-MMP-mediated transcytosis. MT1-NP co-administrated with iRGD exhibited a significantly wider and higher distribution in tumor parenchyma than all the other three formulations (Fig. 9), which was believed to be benefited from the MT1-AF7p-mediated transcytosis and iRGD-facilitated extravasation and tumor penetration.

Extravasation of nanoparticles from blood vessels and accumulation in the tumor site is not the endpoint of the glioma targeted drug delivery, the ultimate step is to penetrate through the multicellular layers of glioma cells and be internalized by more tumor cells to achieve higher anti-glioma efficiency [9]. *In vitro* 3D tumor spheroids provide an important link between monolayer cell cultures and animal experiments for evaluating drug delivery efficiency [48,49]. Tumor spheroids generated by liquid overlay technique not only contain aggregates of cells in close contact but also an organized extracellular matrix consisting of fibronectin, laminin, collagen, and GAG, similar with the extracellular matrix of tumors *in vivo* [50]. Thereby, C6 glioma spheroid served as an appropriate model to evaluate the interstitial penetration and diffusion of MT1-NP. It was found that the glioma penetration ability of MT1-NP was much higher than that of NP (Fig. 6B, C), indicating that MT1-AF7p peptide itself could facilitate nanoparticles penetration inside the glioma spheroids. This efficient transport was also confirmed by the growth inhibition experiments, in which MT1-NP-PTX exhibited the most significant inhibition to the growth of glioma spheroids (Fig. 7A, B).

In the survival study, the MT1-NP-PTX and iRGD combination regimen resulted in the longest survival of mice (Fig. 10). The likely reason underlying the observed remarkable prolonged survival is that MT1-AF7p functionalization and iRGD co-administration facilitate the accumulation of more nanoparticles in the tumor site, and the MT1-AF7p functionalization further drive nanoparticles internalization into glioma cells. Although *in vivo* glioma distribution showed that MT1-NP displayed a glioma distribution profile comparable to that of NP with co-administration of iRGD (Fig. 9), MT1-NP-PTX significantly prolonged animal survival when compare with NP-PTX with co-administration of iRGD peptide. This result was in good consistent with the data of inhibition of tumor spheroid growth and further confirmed that actively dual-targeted MT1-NP demonstrated advantage over passive targeting NP in anti-glioma therapy.

5. Conclusion

Co-administration of MT1-AF7p-conjugated PEG-PLA nanoprticles with a tumor penetrating peptide iRGD was proposed here for facilitating efficient anti-glioblastoma drug delivery. After modification with MT1-AF7p, PEG-PLA nanoparticles displayed a uniformly spherical shape with particle size of 131.33 ± 4.94 nm. MT1-AF7p-conjugated PEG-PLA nanoparticles displayed higher cell association in C6 glioma cells, were internalized via energy-dependent macropinocytosis and lipid raft-mediated endocytosis, and improved the anti-proliferation and apoptosis–induction activity of the loaded PTX. *In vivo* imaging and glioma distribution together confirmed that MT1-AF7p functionalization and iRGD co-administration significantly increased the extravasation of nanoparticles from the BTB and accumulation in the glioma parenchyma. Furthermore, *in vitro* C6 glioma spheroid assays showed that MT1-NP effectively penetrated into the glioma spheroids and significantly improved the inhibitory effects of PTX on the growth of glioma spheroids. With these outstanding properties, MT1-NP-PTX co-administrated with iRGD achieved the longest survival in mice bearing intracranial C6 glioma. These findings indicated that the BTB/glioma cells dual-targeting DDS co-administrated with iRGD peptide might provide a feasible solution for efficient anti-glioblastoma drug delivery.

Acknowledgments

This work was supported by National Key Basic Research Program (2013CB932502), National Natural Science Foundation of China (81072592), National Science and Technology major Project (2012ZX09304004), Innovation Program of Shanghai Municipal

Education Commission (12ZZ107), Program for New Century Excellent Talents in University and Grants from Shanghai Science and Technology Committee (11430702200, 12ZR1416300 and 12nm0502000). The authors also acknowledge the support from School of Pharmacy, Fudan University & the Open Project Program of Key Lab of Smart Drug Delivery (Fudan University), Ministry of Education & PLA, China (2011SDD-10).

References

[1] Stupp R, Mason WP, van den Bent MJ, Weller M, Fisher B, Taphoorn MJ, et al. Radiotherapy plus concomitant and adjuvant temozolomide for glioblastoma. N Engl J Med 2005;352:987–96.
[2] Nduom EK, Bouras A, Kaluzova M, Hadjipanayis CG. Nanotechnology applications for glioblastoma. Neurosurg Clin N Am 2012;23:439–49.
[3] Liu S, Guo Y, Huang R, Li J, Huang S, Kuang Y, et al. Gene and doxorubicin co-delivery system for targeting therapy of glioma. Biomaterials 2012;33:4907–16.
[4] Agarwal S, Sane R, Oberoi R, Ohlfest JR, Elmquist WF. Delivery of molecularly targeted therapy to malignant glioma, a disease of the whole brain. Expert Rev Mol Med 2011;13:e17.
[5] Lawson HC, Sampath P, Bohan E, Park MC, Hussain N, Olivi A, et al. Interstitial chemotherapy for malignant gliomas: the Johns Hopkins experience. J Neurooncol 2007;83:61–70.
[6] Jain RK, di Tomaso E, Duda DG, Loeffler JS, Sorensen AG, Batchelor TT. Angiogenesis in brain tumours. Nat Rev Neurosci 2007;8:610–22.
[7] Zhan C, Meng Q, Li Q, Feng L, Zhu J, Lu W. Cyclic RGD-polyethylene glycol-polyethylenimine for intracranial glioblastoma-targeted gene delivery. Chem Asian J 2012;7:91–6.
[8] Xie H, Xue YX, Liu LB, Liu YH. Endothelial-monocyte-activating polypeptide II increases blood-tumor barrier permeability by down-regulating the expression levels of tight junction associated proteins. Brain Res 2010;1319:13–20.
[9] Minchinton AI, Tannock IF. Drug penetration in solid tumours. Nat Rev Cancer 2006;6:583–92.
[10] Grantab R, Sivananthan S, Tannock IF. The penetration of anticancer drugs through tumor tissue as a function of cellular adhesion and packing density of tumor cells. Cancer Res 2006;66:1033–9.
[11] Phillips RM, Loadman PM, Cronin BP. Evaluation of a novel in vitro assay for assessing drug penetration into avascular regions of tumours. Br J Cancer 1998;77:2112–9.
[12] Rozhkova EA. Nanoscale materials for tackling brain cancer: recent progress and outlook. Adv Mater 2011;23:H136–50.
[13] Orringer DA, Koo YE, Chen T, Kopelman R, Sagher O, Philbert MA. Small solutions for big problems: the application of nanoparticles to brain tumor diagnosis and therapy. Clin Pharmacol Ther 2009;85:531–4.
[14] Beduneau A, Saulnier P, Benoit JP. Active targeting of brain tumors using nanocarriers. Biomaterials 2007;28:4947–67.
[15] Guo J, Gao X, Su L, Xia H, Gu G, Pang Z, et al. Aptamer-functionalized PEG-PLGA nanoparticles for enhanced anti-glioma drug delivery. Biomaterials 2011;32:8010–20.
[16] Zhan C, Gu B, Xie C, Li J, Liu Y, Lu W. Cyclic RGD conjugated poly(ethylene glycol)-co-poly(lactic acid) micelle enhances paclitaxel anti-glioblastoma effect. J Control Release 2010;143:136–42.
[17] Forsyth PA, Wong H, Laing TD, Rewcastle NB, Morris DG, Muzik H, et al. Gelatinase-A (MMP-2), gelatinase-B (MMP-9) and membrane type matrix metalloproteinase-1 (MT1-MMP) are involved in different aspects of the pathophysiology of malignant gliomas. Br J Cancer 1999;79:1828–35.
[18] Nakada M, Kita D, Futami K, Yamashita J, Fujimoto N, Sato H, et al. Roles of membrane type 1 matrix metalloproteinase and tissue inhibitor of metalloproteinases 2 in invasion and dissemination of human malignant glioma. J Neurosurg 2001;94:464–73.
[19] Deryugina EI, Soroceanu L, Strongin AY. Up-regulation of vascular endothelial growth factor by membrane-type 1 matrix metalloproteinase stimulates human glioma xenograft growth and angiogenesis. Cancer Res 2002;62:580–8.
[20] Munaut C, Noel A, Hougrand O, Foidart JM, Boniver J, Deprez M. Vascular endothelial growth factor expression correlates with matrix metalloproteinases MT1-MMP, MMP-2 and MMP-9 in human glioblastomas. Int J Cancer 2003;106:848–55.
[21] Belien AT, Paganetti PA, Schwab ME. Membrane-type 1 matrix metalloprotease (MT1-MMP) enables invasive migration of glioma cells in central nervous system white matter. J Cell Biol 1999;144:373–84.
[22] Fillmore HL, VanMeter TE, Broaddus WC. Membrane-type matrix metalloproteinases (MT-MMPs): expression and function during glioma invasion. J Neurooncol 2001;53:187–202.
[23] Nakada M, Okada Y, Yamashita J. The role of matrix metalloproteinases in glioma invasion. Front Biosci 2003;8:e261–9.
[24] Zhu L, Wang H, Wang L, Wang Y, Jiang K, Li C, et al. High-affinity peptide against MT1-MMP for in vivo tumor imaging. J Control Release 2011;150:248–55.
[25] Lammers T, Kiessling F, Hennink WE, Storm G. Drug targeting to tumors: principles, pitfalls and (pre-) clinical progress. J Control Release 2012;161:175–87.
[26] Heldin CH, Rubin K, Pietras K, Ostman A. High interstitial fluid pressure – an obstacle in cancer therapy. Nat Rev Cancer 2004;4:806–13.
[27] Lee H, Fonge H, Hoang B, Reilly RM, Allen C. The effects of particle size and molecular targeting on the intratumoral and subcellular distribution of polymeric nanoparticles. Mol Pharm 2010;7:1195–208.
[28] Sugahara KN, Teesalu T, Karmali PP, Kotamraju VR, Agemy L, Girard OM, et al. Tissue-penetrating delivery of compounds and nanoparticles into tumors. Cancer Cell 2009;16:510–20.
[29] Sugahara KN, Teesalu T, Karmali PP, Kotamraju VR, Agemy L, Greenwald DR, et al. Coadministration of a tumor-penetrating peptide enhances the efficacy of cancer drugs. Science 2010;328:1031–5.
[30] Bello L, Francolini M, Marthyn P, Zhang J, Carroll RS, Nikas DC, et al. Alpha(v)beta3 and alpha(v)beta5 integrin expression in glioma periphery. Neurosurgery 2001;49:380–9. 390.
[31] Ding H, Wu X, Roncari L, Lau N, Shannon P, Nagy A, et al. Expression and regulation of neuropilin-1 in human astrocytomas. Int J Cancer 2000;88:584–92.
[32] Xia H, Gao X, Gu G, Liu Z, Zeng N, Hu Q, et al. Low molecular weight protamine-functionalized nanoparticles for drug delivery to the brain after intranasal administration. Biomaterials 2011;32:9888–98.
[33] Gu G, Xia H, Hu Q, Liu Z, Jiang M, Kang T, et al. PEG-co-PCL nanoparticles modified with MMP-2/9 activatable low molecular weight protamine for enhanced targeted glioblastoma therapy. Biomaterials 2013;34:196–208.
[34] Zeng N, Gao X, Hu Q, Song Q, Xia H, Liu Z, et al. Lipid-based liquid crystalline nanoparticles as oral drug delivery vehicles for poorly water-soluble drugs: cellular interaction and in vivo absorption. Int J Nanomedicine 2012;7:3703–18.
[35] Hu Q, Gu G, Liu Z, Jiang M, Kang T, Miao D, et al. F3 peptide-functionalized PEG-PLA nanoparticles co-administrated with tLyp-1 peptide for anti-glioma drug delivery. Biomaterials 2013;34:1135–45.
[36] Yu DH, Lu Q, Xie J, Fang C, Chen HZ. Peptide-conjugated biodegradable nanoparticles as a carrier to target paclitaxel to tumor neovasculature. Biomaterials 2010;31:2278–92.
[37] Ulrich TA, Jain A, Tanner K, MacKay JL, Kumar S. Probing cellular mechanobiology in three-dimensional culture with collagen-agarose matrices. Biomaterials 2010;31:1875–84.
[38] Jiang X, Xin H, Gu J, Xu X, Xia W, Chen S, et al. Solid tumor penetration by integrin-mediated pegylated poly(trimethylene carbonate) nanoparticles loaded with paclitaxel. Biomaterials 2013;34:1739–46.
[39] Allard E, Passirani C, Benoit JP. Convection-enhanced delivery of nanocarriers for the treatment of brain tumors. Biomaterials 2009;30:2302–18.
[40] Norden AD, Drappatz J, Wen PY. Antiangiogenic therapies for high-grade glioma. Nat Rev Neurol 2009;5:610–20.
[41] Hu K, Li J, Shen Y, Lu W, Gao X, Zhang Q, et al. Lactoferrin-conjugated PEG-PLA nanoparticles with improved brain delivery: in vitro and in vivo evaluations. J Control Release 2009;134:55–61.
[42] Pellet-Many C, Frankel P, Jia H, Zachary I. Neuropilins: structure, function and role in disease. Biochem J 2008;411:211–26.
[43] Alexis F, Pridgen E, Molnar LK, Farokhzad OC. Factors affecting the clearance and biodistribution of polymeric nanoparticles. Mol Pharm 2008;5:505–15.
[44] Song Q, Yao L, Huang M, Hu Q, Lu Q, Wu B, et al. Mechanisms of transcellular transport of wheat germ agglutinin-functionalized polymeric nanoparticles in Caco-2 cells. Biomaterials 2012;33:6769–82.
[45] Xia H, Gao X, Gu G, Liu Z, Hu Q, Tu Y, et al. Penetratin-functionalized PEG-PLA nanoparticles for brain drug delivery. Int J Pharm 2012;436:840–50.
[46] Vercauteren D, Vandenbroucke RE, Jones AT, Rejman J, Demeester J, De Smedt SC, et al. The use of inhibitors to study endocytic pathways of gene carriers: optimization and pitfalls. Mol Ther 2010;18:561–9.
[47] Nakase I, Niwa M, Takeuchi T, Sonomura K, Kawabata N, Koike Y, et al. Cellular uptake of arginine-rich peptides: roles for macropinocytosis and actin rearrangement. Mol Ther 2004;10:1011–22.
[48] Mehta G, Hsiao AY, Ingram M, Luker GD, Takayama S. Opportunities and challenges for use of tumor spheroids as models to test drug delivery and efficacy. J Control Release 2012;164:192–204.
[49] Pampaloni F, Reynaud EG, Stelzer EH. The third dimension bridges the gap between cell culture and live tissue. Nat Rev Mol Cell Biol 2007;8:839–45.
[50] Xin H, Sha X, Jiang X, Zhang W, Chen L, Fang X. Anti-glioblastoma efficacy and safety of paclitaxel-loading angiopep-conjugated dual targeting PEG-PCL nanoparticles. Biomaterials 2012;33:8167–76.